Draft version February 27, 2015
Preprint typeset using LaTeX style emulateapj v. 5/2/11

arXiv:1412.1100v2 [astro-ph.GA] 25 Feb 2015

SIMULATIONS OF GALAXIES FORMED IN WARM DARK MATTER HALOS OF MASSES AT THE FILTERING SCALE

P. Colín[1], V. Avila-Reese[2], A. González-Samaniego[2], H. Velázquez[3]

Draft version February 27, 2015

ABSTRACT

We present zoom-in N-body + Hydrodynamic simulations of dwarf central galaxies formed in Warm Dark Matter (WDM) halos with masses at present-day of $2-4\times10^{10}$ $M_\odot$. Two different cases are considered, the first one when halo masses are close to the corresponding half-mode filtering scale, M_f ($m_{\rm WDM}$=1.2 keV) and the second when they are 20 to 30 times the corresponding M_f ($m_{\rm WDM}$= 3.0 keV). The WDM simulations are compared with the respective Cold Dark Matter (CDM) simulations. The dwarfs formed in halos of masses $(20-30)M_f$ have roughly similar properties and evolution than their CDM counterparts; on the contrary, those formed in halos of masses around M_f, are systematically different from their CDM counterparts. As compared to the CDM dwarfs, they assemble the dark and stellar masses later, having mass-weighted stellar ages 1.4–4.8 Gyr younger; their circular velocity profiles are shallower, with maximal velocities 20–60% lower; their stellar distributions are much less centrally concentrated and with larger effective radii, by factors 1.3–3. The WDM dwarfs at the filtering scale ($m_{\rm WDM}$=1.2 keV) have disk-like structures, and end in most cases with higher gas fractions and lower stellar-to-total mass ratios than their CDM counterparts. The late halo assembly, low halo concentrations, and the absence of satellites of the former with respect to the latter, are at the basis of the differences.

Subject headings: cosmology:dark matter — galaxies:dwarfs — galaxies:formation — methods:N-body simulations — methods: Hydrodynamics

1. INTRODUCTION

The Λ cold dark matter (ΛCDM) cosmology provides the most accepted background for studying the process of cosmic structure formation in the Universe. The predictions of the ΛCDM-based scenario of structure formation are fully consistent with observations of the large-scale structure of the present and past Universe, including the anisotropies in the cosmic microwave background radiation (see Frenk & White 2012, for a review). However, doubts have been cast on whether observations of matter distribution at small –dwarf galactic and subgalactic– scales are consistent with the predictions of the ΛCDM scenario (see for recent reviews e.g., Weinberg et al. 2013; Del Popolo et al. 2014). Currently, it is matter of great debate whether the potential problems are real or consequence of observational biases and/or still poorly understood astrophysical processes at small scales. If they are confirmed, introducing variations to the ΛCDM cosmology will appear as a feasible solution.

From the point of view of initial conditions for the cosmic structure formation, ΛCDM is the simplest model. For the ΛCDM model: (1) the cut-off scale in the linear mass power spectrum of perturbations due to free streaming, $\lambda_{\rm fs}$, is many orders of magnitude smaller than the resolution reached by current numerical cosmological simulations of galactic halos so that in practice $\lambda_{\rm fs}=0$ and hierarchical cosmic structure formation proceeds at all scales; (2) the relic thermal velocities of the CDM particles, $v_{\rm th}$, are very small, so in practice $v_{\rm th}$=0 is assumed; (3) since CDM particles are non-baryonic, they do not interact electromagnetically, and are assumed to have a negligible self-interaction cross section, $\sigma_{\rm SI}=0$, constituting the CDM in practice a pure collisionless fluid; and (4) the statistical distribution of the primordial overdensity perturbations is assumed to be Gaussian. Therefore, the relaxation of any of the above listed assumptions implies necessarily the introduction of free parameters in the initial conditions of cosmic structure formation as would be $\lambda_{\rm fs}$, $v_{\rm th}$, $\sigma_{\rm SI}$, or the skewness and kurtosis in the primordial density perturbations distribution.

More than a decade ago, high-resolution N-body cosmological simulations were performed to explore how substructure, inner density profiles and shapes of halos were affected when one or several of the ΛCDM assumptions listed above were relaxed. Specifically, in these simulations were introduced: (a) a cut-off in the power spectrum and/or non-negligible thermal velocities in the dark particles (in concordance with the Λ warm dark matter, ΛWDM, cosmology; Colín et al. 2000; Avila-Reese et al. 2001; see also, Bode et al. 2001, Knebe et al. 2002); (b) a non-negligible self-interaction with constant and velocity-dependent particle cross sections (Yoshida et al. 2000; Colín et al. 2002, see also Spergel & Steinhardt 2000; Firmani et al. 2000); (c) and non-Gaussian initial perturbations, positively or negatively skewed (Avila-Reese et al. 2003).

Among alternative cosmologies, the most popular is the ΛWDM one with a power spectrum filtered at scales corresponding to dwarf galaxies. As N-body simulations show, in this case the amount of substructure in Milky Way-sized halos is considerably reduced (e.g., Colín et al. 2000; Bode et al. 2001; Knebe et al. 2002; Macciò & Fontanot 2010; Kennedy et al. 2014),

[1] Centro de Radioastronomía y Astrofísica, Universidad Nacional Autónoma de México, A.P. 72-3 (Xangari), Morelia, Michoacán 58089, México
[2] Instituto de Astronomía, Universidad Nacional Autónoma de México, A.P. 70-264, 04510, México, D.F., México
[3] Instituto de Astronomía, Universidad Nacional Autónoma de México, Apdo. Postal 877, Ensenada, BC, CP 22830, México

the abundance of low-circular velocity halos hosting dwarf galaxies is lowered (e.g., Zavala et al. 2009; Papastergis et al. 2011), and, although the halos/subhalos do not present shallow cores at the scales of astrophysical interest, they are less concentrated and with lower maximum circular velocities than their CDM counterparts (Avila-Reese et al. 2001; Colín et al. 2008; Lovell et al. 2012; Schneider et al. 2012; Anderhalden et al. 2013). These and other effects make the ΛWDM model an appealing alternative for alleviating the potential problems of the ΛCDM model at small scales, while conserving its successes at larger scales.

The main constraint to the ΛWDM scenario comes from the comparison of the results of WDM hydrodynamic simulations in the quasi-linear regime with the Ly-α flux power spectrum of high-redshift quasars (Narayanan et al. 2000; Viel et al. 2005), though these comparisons are not free of uncertainties and limitations (see e.g., de Vega et al. 2014). Depending on the nature of the WDM particle, thermal, sterile neutrino, etc., a lower limit to its mass, $m_{\rm WDM}$, can be established from the Ly-α forest analysis, which implies an upper limit to the damping scale in the mass power spectrum. Several updated estimates were presented recently in the literature (e.g., Viel et al. 2013). Based on the constrains of the latter authors (for a thermal relic particle, $m_{\rm WDM}$ should be $\gtrsim$ 3.3 keV at the 2σ level), Schneider et al. (2014) conclude that the upper limit in the damping is at so small scales that the allowed ΛWDM models would not be already able to solve the potential problems of ΛCDM.

So far, most studies on galaxy properties in the ΛWDM scenario were based on dark-matter-only simulations or a combination of these kind of simulations with semi-analytic models (for the latter see e.g., Macciò & Fontanot 2010; Menci et al. 2012; Kang et al. 2013). However, by their own nature, these approaches can not take into account the effects of the non-linear baryonic physics on the evolution and dynamics of the halos, which can be important. Thus, inferences based on the analysis of dark-matter-only simulations (and, perhaps, semi-analytic models) are necessarily limited when comparing with observations (see e.g. Kang et al. 2013). It is then important to go beyond those techniques and perform full N-body + Hydrodynamics simulations. An interesting question than one can ask is how much differ the evolution and properties of galaxies formed in the ΛWDM scenario from those formed in the ΛCDM one. At this point, it is important to recognize that the dark-matter structure evolution is expected to be very similar in both scenarios at scales much larger than the filtering one, with differences appearing gradually at scales approaching this scale.

The so-called half-mode wavelength or its corresponding mass, M_f, is commonly chosen as the relevant *filtering* scale at which WDM halo abundance and properties start to significantly deviate from the CDM case (see for the exact definition and references Section 2). In this paper, we present a set of zoom-in N-body + Hydrodynamics simulations of (dwarf) galaxies formed in WDM scenario in halos with masses $\lesssim M_f$ and $20-30M_f$, and compare them with their CDM counterparts. Recently, Herpich et al. (2014, see also Libeskind et al. 2013) reported WDM simulations of this kind but for three halos of masses significantly larger than the filtering masses corresponding to their WDM particle masses ($m_{\rm WDM}$= 1, 2, and 5 keV). This is very likely the reason why the evolution of their WDM galaxies did not differ significantly from the CDM counterparts. After completion of our study, it appeared a preprint by Governato et al. (2014), where the authors present a simulation of *one* dwarf galaxy formed in a $\sim 10^{10}$ M$_\odot$ halo, both in WDM and CDM cosmologies. For the WDM cosmology, $m_{\rm WDM}$=2 keV was used, which implies that their system is ~ 2 times larger than the filtering mass.

Here, our goal is to explore the evolution and properties of dwarf galaxies formed in *halos of masses similar to* the filtering mass M_f that corresponds to a thermal WDM particle mass of 1.2 keV. These are expected to be among the most abundant halos in this WDM scenario; below $\sim 0.5M_f$, the halo mass function strongly decreases, and the structures, rather than virialized halos, are isolated 3D enhancements not assembled hierarchically (Angulo et al. 2013). The evolution and properties of the galaxy-halo systems around the filtering mass *might in several aspects be generic regardless of the value of this mass*; though, astrophysical processes such as stellar feedback and reionization could make the extrapolation of our results to other filtering or thermal WDM particle masses inadequate.

In Section 2, the cosmological background and the used WDM models are presented. The details of the code and simulations performed here are given in Section 3. The properties and evolution of the simulated WDM dwarf galaxies and their corresponding CDM ones are presented in Section 4. A summary of the results and further discussion are presented in Section 5.

2. THE COSMOLOGICAL MODELS

The cosmological background used in our numerical simulations is a flat, low-density model with $\Omega_m = 0.3$, $\Omega_b = 0.045$, $\Omega_\Lambda = 0.7$, and $h = 0.7$. For the CDM initial power spectrum, $P(k)_{CDM}$, we adopt the approximation by Klypin & Holtzman (1997), which was obtained as a direct fit of the power spectrum calculated using a Boltzmann code. For the scales studied in this paper, and even larger ones, this approximation is very accurate. In the case of WDM, the power spectrum at large scales is essentially that of the CDM, but at small scales the power is systematically reduced due to the free-streaming damping. The transfer function $T^2_{WDM}(k)$ describes such a deviation from the CDM power spectrum,

$$P_{WDM}(k) = T^2_{WDM}(k) P_{CDM}(k). \quad (1)$$

The CDM or WDM power spectra are normalized to $\sigma_8 = 0.8$, a value close to that estimated from the *Planck* mission (Planck Collaboration et al. 2014); σ_8 is the rms of $z = 0$ mass perturbations estimated with the top-hat window of radius $8h^{-1}$Mpc.

The free-streaming of collisionless particles erase dark matter perturbations below a scale given by the properties of the dark matter particle. Here, we will refer to the case of fully thermalized particles at decoupling as *thermal relics*. A simple analysis gives an estimate of the comoving length at which thermal particles diffuse out

(e.g., Kolb & Turner 1994; Schneider et al. 2012):

$$\lambda_{fs} \simeq 0.4 \left(\frac{m_{\rm WDM}}{\rm keV}\right)^{-4/3} \left(\frac{\Omega_{WDM} h^2}{0.135}\right)^{1/3} [h^{-1}{\rm M}_\odot]. \quad (2)$$

However, in order to calculate the whole processed power spectrum, the coupled Boltzmann relativistic system of equations for the various species of matter and radiation should be numerically solved. Here, we adopt the WDM transfer function given in Viel et al. (2005):

$$T_{WDM}(k) = \left[1 + (\alpha k)^{2.0\nu}\right]^{-5.0/\nu}, \quad (3)$$

where $\nu = 1.12$ and the parameter α is related to $m_{\rm WDM}$, Ω_{WDM}, and h through

$$\alpha = a \left(\frac{m_{\rm WDM}}{\rm 1keV}\right)^{b} \left(\frac{\Omega_{WDM}}{0.25}\right)^{c} \left(\frac{h}{0.7}\right)^{d} h^{-1}{\rm Mpc}, \quad (4)$$

with $a = 0.049$, $b = -1.11$, $c = 0.11$, $d = 1.22$. In eq. (3), α is a characteristic scale length that can be related to an effective free-streaming scale, $\lambda_{\rm fs}^{\rm eff} \equiv \alpha$ (e.g., Schneider et al. 2012). The corresponding effective free-streaming mass is then:

$$M_{\rm fs} = \frac{4\pi}{3} \bar{\rho} \left(\frac{\lambda_{\rm fs}^{\rm eff}}{2}\right)^3, \quad (5)$$

where $\bar{\rho}$ is the present-day background density. The primordial density perturbations below $M_{\rm fs}$ are expected to be completely erased, while perturbations with masses up to thousand times $M_{\rm fs}$ can be significantly affected by the damping process. It is common, on the other hand, to define a characteristic scale below which the linear WDM power spectrum start to deviate significantly from the CDM one (Sommer-Larsen & Dolgov 2001; Avila-Reese et al. 2001). Following Avila-Reese et al. (2001), we define the half-mode wavenumber, $k_{\rm hm}$, for which $T^2_{WDM}(k) = 0.5$; i.e., where the value of the power spectrum of the WDM model is half that of the corresponding CDM one. The associated half-mode *filtering* mass is given by:

$$M_f = \frac{4\pi}{3} \bar{\rho} \left(\frac{\lambda_{\rm hm}}{2}\right)^3, \quad (6)$$

where $\lambda_{\rm hm} = 2\pi/k_{\rm hm}$ is the comoving half-mode length.[4] This filtering mass scale, which is much larger than $M_{\rm fs}$, is where one expects the abundance and properties of the halos to start to significantly deviate from the CDM case (Colín et al. 2008; Smith & Markovic 2011; Menci et al. 2012; Schneider et al. 2012; Benson et al. 2013; Angulo et al. 2013). At masses around M_f, the abundance of halos already falls below, by a factor of ~ 2, that of the corresponding CDM one, reaching its relatively shallow peak at $\sim 0.5\ M_f$. Thus, the most abundant halos in the WDM cosmogony are those of masses around to M_f.

Structures of masses close to M_f can be unambiguously defined as approximately spherical virialized objects that resemble those seen in CDM simulations, albeit

[4] Note that some authors define the half-mode wavenumber as $T_{WDM}(k) = 0.5$ (e.g., Schneider et al. 2012), which implies a smaller M_f than in our case.

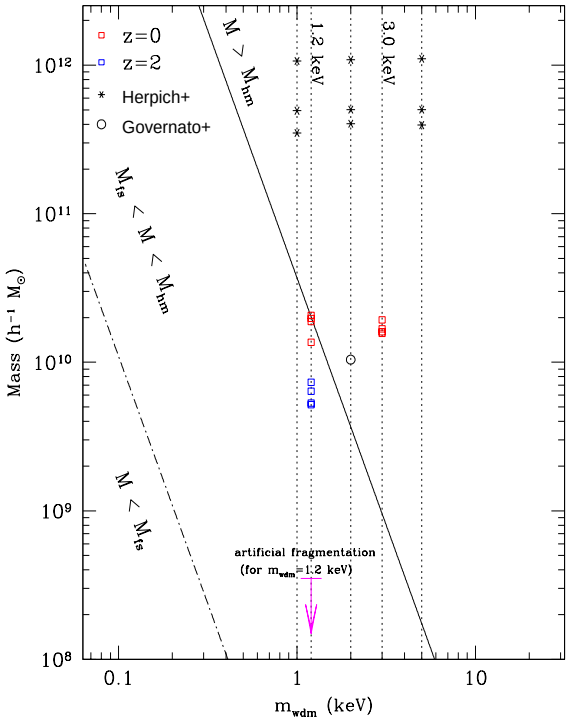

FIG. 1.— The free-streaming and half-mode (filtering) mass scales as a function of the thermal relic particle mass, $m_{\rm WDM}$ (for a sterile neutrino particle, see eq. 7). The squares show where our simulations lie at $z = 0$ (red) and at $z = 2$ (blue; only for the 1.2 keV case). Even at $z = 2$ our simulations are far from the artificial fragmentation scale for a filtering corresponding to 1.2 keV (downwards arrow). The starred symbols and the open circle correspond to the simulations presented in Herpich et al. (2014) and Governato et al. (2014) at $z = 0$.

with some differences; for instance, they are less concentrated (e.g., Avila-Reese et al. 2001; Angulo et al. 2013). Moreover, halos of masses $\gg M_f$ are expected to assemble hierarchically, sharing the same properties as their CDM counterparts. Systems of masses several times smaller than M_f but larger than $M_{\rm fs}$ can be defined as "protohalos", that is halos that are not fully formed, but show clear isolated 3D enhancements (Angulo et al. 2013). At masses close to $M_{\rm fs}$, these authors report structures that appear as clear failures of their halo finder algorithm, these include outer caustics of large halos and dense sheets and filaments, where the collapse of a further axis has just started.

Following Schneider et al. (2014), in Fig. 1, we show the dependence of M_f and $M_{\rm fs}$ on the thermal WDM particle mass $m_{\rm WDM}$. For a given $m_{\rm WDM}$ and at any epoch, objects located well above the solid line ($M = M_f$) are halos assembled hierarchically, as in the CDM cosmogony. Objects of masses close to M_f, on the other hand, can be considered "normal" halos. However, their early assembly is already affected by the filtering at small scales; for example, they form later than their CDM counterparts. The objects that Angulo et al. (2013) define as "protohalos" start to apear as the mass decreases below M_f and dominate the population when $M \ll M_f$. In these "protohalos", the hierarchical assembly fails notoriously (e.g.,

Schneider et al. 2012). Finally, below the dot-dashed line ($M = M_{\rm fs}$), no structure formation is expected. However, in N-body simulations it is possible to find structures smaller than $M_{\rm fs}$ but they are actually artificial (see e.g., Avila-Reese et al. 2001; Bode et al. 2001; Götz & Sommer-Larsen 2003; Knebe et al. 2003; Wang & White 2007; Schneider et al. 2013; Angulo et al. 2013).

In Fig. 1 we plot our eight simulated systems (presented below) with red squares as well as those simulated by Herpich et al. (2014) and Governato et al. (2014), starred and open circle symbols (their M_{200} masses were multiplied by 1.24 so as to take into account our different definition of virial mass). These masses are at $z = 0$; we also plot the virial masses of our simulated systems at $z = 2$ (blue squares). The downwards arrow indicates the mass scale where spurious structures would form in our simulations with $m_{\rm WDM}$=1.2 keV (for $m_{\rm WDM}$=3 keV, it is at a smaller mass) due to numerical fragmentation, according to the criterion given by Wang & White (2007). This criterion depends on the filtering scale and the resolution of the numerical simulation. As can be seen, our halos lie above the downwards arrow even at $z = 2$. Yet, it might be that numerical artifacts are present at the highest redshifts, when the progenitor masses are very small.

The relations show in Fig. 1 are for thermal relic particles. Popular candidates for WDM are also the sterile and right-handed neutrinos, particles proposed to never been in thermal equilibrium (Dodelson & Widrow 1994; Shi & Fuller 1999; Abazajian et al. 2001; see Boyarsky et al. 2009 for a review). Viel et al. (2005) provided a relation between the non-resonantly produced sterile neutrino mass and the mass of the thermal relic particle such that the transfer function for this kind of sterile neutrino can be calculated according to eq. (3). The relation is given by

$$m_{\nu_s} = 4.43 \text{ keV}(m_{\rm WDM}/1 \text{ keV})^{4/3}(\Omega_{WDM}h^2)^{-1/3}. \quad (7)$$

Thus, for a given cosmological background, we can use Fig. 1 also for the case of the non-resonantly produced sterile neutrino, after going from $m_{\rm WDM}$ to m_{ν_s}. Another particle candidate for WDM is the gravitino (e.g., Pagels & Primack 1982; Ellis et al. 1984; Moroi et al. 1993). Weakly interacting massive particles (WIMPs, the most favored candidates for CDM), if produced in non-thermal processes, can also have large free-streaming lengths and emulate the power spectrum of WDM (e.g., Lin et al. 2001; He & Lin 2013).

Finally, thermal WDM particles are expected to have a relic velocity dispersion, which could affect the inner structure of halos due to the Liouville theorem limit for the phase density (Hogan & Dalcanton 2000). However, this velocity dispersion is very small for reasonable mass candidates (~ 3.0 keV) and even for thermal particle masses as low as $m_{\rm WDM} \sim 1$ keV it does not affect significantly the inner structure of WDM halos (Avila-Reese et al. 2001; Colín et al. 2008; Macciò et al. 2012). Therefore, we assume a zero thermal velocity dispersion, $v_{\rm th}$=0, in our simulations.

3. THE CODE AND THE SIMULATIONS

We have carried out a set of N-body + Hydrodynamics simulations of low-mass halos using the zoom-in technique in both the ΛWDM cosmology and its counterpart the ΛCDM one. The simulations were run using the Adaptive Refinement Tree (ART) N-body/hydrodynamic code (Kravtsov et al. 1997, 2003). The code includes gas cooling, star formation (SF), stellar feedback, advection of metals, and a UV heating background source. The cooling and heating rates incorporate Compton heating/cooling, atomic and molecular cooling, UV heating from a cosmological background radiation (Haardt & Madau 1996), and are tabulated for a temperature range of $10^2 < T < 10^9$ K and a grid of densities, metallicities, and redshifts using the CLOUDY code (Ferland et al. 1998, version 96b4).

The SF and feedback processes (subgrid physics) are implemented in the code as discussed in detail in Colin et al. (2010) and Avila-Reese et al. (2011). For completeness, they are briefly summarized below. The SF takes place in those cells for which $T < T_{\rm SF}$ and $\rho_g > \rho_{\rm SF}$, where T and ρ_g are the temperature and density of the gas, respectively, and $T_{\rm SF}$ and $\rho_{\rm SF}$ are the temperature and density threshold, respectively. Here, we use the same values of the $T_{\rm SF}$ and $n_{\rm SF}$ parameters as in Avila-Reese et al. (2011); namely, 9000 K and 6 cm^{-3}, respectively, where $n_{\rm SF}$ is the density threshold in hydrogen atoms per cubic centimeter; see Avila-Reese et al. (2011), as well as Colin et al. (2010) and González-Samaniego et al. (2014) (hereafter G+2014), for a discussion on the choice of these values, in particular $n_{\rm SF}$. A stellar particle of mass $m_* = \epsilon_{\rm SF}\, m_g$ is placed in a grid cell every time the above conditions are simultaneously satisfied, where m_g is the gas mass in the cell and $\epsilon_{\rm SF}$ is a parameter that measures the local efficiency by which gas is converted into stars. As in Avila-Reese et al. (2011), we set $\epsilon_{\rm SF} = 0.5$.

We use the "explosive" stellar thermal feedback recipe, according to which each star more massive than 8 M$_\odot$ injects instantaneously into the cell, where the particle is located, $E_{\rm SN+Wind} = 2 \times 10^{51}$ erg of *thermal* energy; half of this energy is assumed to come from the type-II SN and half from the shocked stellar winds. This energy provided by the stellar feedback raises the temperature of the cell to values $\gtrsim 10^7$ K; the precise value depends on the assumed initial mass function (IMF), the amount of energy assumed to be dumped by each massive star, and the value of the $\epsilon_{\rm SF}$ parameter. On the other hand, each 8M$_\odot$ ejects 1.3M$_\odot$ of metals. For the assumed Miller & Scalo (1979) IMF, a stellar particle of 10^5 M$_\odot$ produces 749 type-II SNe.

In our previous works, we have delayed the radiative cooling for some time (typically between 10 and 40 Myr) in those cells where young stellar particles are, in order to avoid overcooling due to, for instance, resolution limitations. However, at the current resolution reached by our simulations and for the typical densities found in the SF cells (~ 10 cm^{-3}), which in turn depend on $n_{\rm SF}$, the cooling time is actually much larger than the crossing time (Dalla Vecchia & Schaye 2012). Thus, for the simulations used in this study, switching-off the cooling temporarily is expected to have only a minor effect on the properties of the simulated galaxies. We have carried out some tests and verified that this is the case. However, we

decided to keep in the code this cooling delay when running the ΛWDM simulations because some of the corresponding CDM galaxies, to be compared with the WDM ones, were run with this prescription (G+2014).

3.1. *The zoom-in simulations*

The aim of this paper is to explore the evolution of galaxies formed in WDM halos of masses around the half-mode (filtering) scale M_f. As discussed in Section 2, M_f is a characteristic scale, where the properties and abundance of the WDM halos start to depart significantly from those of their CDM counterparts.

Here, we will study one particular value of M_f, corresponding to dwarf-galaxy scales. At a qualitative level, the results might apply to other values of M_f.

According to eqs. (6) and (3), a half-mode mass of $2 \times 10^{10}\ h^{-1}\mathrm{M}_\odot$ is associated to a thermal relic particle of $m_{\rm WDM} = 1.2$ keV (see Fig. 1). In G+2014, a set of seven zoom-in ΛCDM N-body+ Hydrodynamics simulations that end up with around this mass were analyzed with the purpose of exploring the effects of different halo mass assembly histories (MAHs) on the evolution and properties of central dwarf galaxies. These low-mass simulated galaxies have enough resolution (see below) so that an analysis of their internal structural properties can be done with some confidence. Therefore, in order to study systems at the half-mode mass scale and compare them with the CDM results, we carry out here zoom-in simulations of some of the G+2014 runs but using the WDM power spectrum corresponding to $m_{\rm WDM} = 1.2$ keV (case $\mathrm{WDM}_{1.2}$ hereafter). We also carry out simulations of the same systems for a WDM power spectrum corresponding to $m_{\rm WDM} = 3$ keV (case $\mathrm{WDM}_{3.0}$ hereafter), in order to explore whether the properties of simulated galaxies in halos much more massive than M_f tend to be similar to those of galaxies formed in CDM halos. For this case, $M_f = 9.6 \times 10^8\ h^{-1}\mathrm{M}_\odot$ and thus, the simulated systems are about 20-30 times M_f.

The ΛWDM simulations performed here have the same random seed and box size as the ΛCDM simulations in G+2014. Therefore, all the target WDM halos/galaxies here have their CDM counterpart simulations. The box used in G+2014 has $L_{box} = 10\ h^{-1}$Mpc per side and a root grid of 128^3 cells. We first set the multiple-mass species initial conditions with the code PMstartM (Klypin et al. 2001) and then run a low–mass resolution simulation with the N-body ART code (Kravtsov et al. 1997). A spherical region of radius three times the virial radius $R_{\rm v}$ of the selected halo is chosen. The virial radius is defined as the radius that encloses a mean density equal to Δ_{vir} times the mean density of the universe, where Δ_{vir} is obtained from the spherical top-hat collapse model. The Lagrangian region corresponding to the $z = 0$ spherical volume is identified at $z = 50$ and resampled with additional small-scale waves (Klypin et al. 2001). The new zoom-in simulation is then run with the hydrodynamic/N-body version of ART. The number of DM particles in the high-resolution zone changes from halo to halo but it is between 500 thousand and one million. The mass per particle m_p in the highest resolution region is $6.6 \times 10^4\ h^{-1}\mathrm{M}_\odot$ and increases for the DM N-body only runs to $7.8 \times 10^4\ h^{-1}\mathrm{M}_\odot$.

In ART, the grid is refined recursively as the matter distribution evolves. The runs use a DM or gas density criteria to refine. In the CDM runs presented in G+2014, the cell is refined when its mass in DM exceeds $1.3\ m_p$ or the mass in gas is higher than $1.4 F_U m_p$, where $F_U \equiv \Omega_b/\Omega_m$ is the universal baryon fraction. For the WDM runs, we have decided to use a less aggressive refinement (it acts as a softening of very small structures) in an attempt to eliminate artificial fragments[5], which are known to arise due to the finite number of particles and the resolved cut-off of the power spectrum (see above for references). Thus, we refine cells only until they reach a mass eight times the previous value of $1.3\ m_p$ in DM or $1.4 F_U m_p$ in gas. To make sure that the less aggressive refinement does not introduce significant differences in the simulations, we resimulated some of the CDM runs with the less aggressive refinement setting. A comparison between the CDM halos/galaxies obtained with the aggressive and soft refinements was done for some of the dwarfs and roughly the same evolution and properties were obtained. In the Appendix, we show and discuss the case for run Dw3.

As in G+2014, in the hydrodynamic simulations presented in this paper, the root grid of 128^3 cubic cells is immediately refined unconditionally to the third level, corresponding to an effective grid size of 1024^3. Although we formally set the maximum refinement level to 11, which implies a minimum cell size of 55 comoving pc, this is not reached in practice in the WDM runs with $m_{\rm WDM} = 1.2$ keV. In general, the number of cells inside $R_{\rm v}$ depends on the mass of the halo/galaxy, cosmology, and on the kind of refinement that was used, but it is roughly about one million and reduces by a factor of eight or so for the less aggressive refinement.

As mentioned above, our study is focused on dwarfs formed in WDM halos that at $z = 0$ have masses close to M_f and much larger than M_f, and on comparing them with their CDM counterparts. From G+2014 we have selected the CDM systems named there as Dw3, Dw4, Dw5 and Dw7, each one with a different halo MAH but with about the same present-day virial masses, $M_{\rm v} = 1.5 - 3 \times 10^{10}\ h^{-1}\mathrm{M}_\odot$. Unfortunately, the halo finder[6] could not identify the halos corresponding to dwarfs Dw4 and Dw7 in the WDM simulation with $m_{\rm WDM} = 1.2$ keV. Hence, only the systems Dw3 and Dw5 have been simulated in all cosmologies: CDM and WDM with $m_{\rm WDM} = 1.2$ and 3 keV. The systems Dw4 and Dw7 were run in WDM with $m_{\rm WDM} = 3$ keV, in which case the corresponding M_f is much smaller than the masses of the simulated objects. In order to have more WDM systems of masses around M_f, we have identified in the 1.2 keV WDM box two more distinct halos, around these masses, and performed the corresponding zoom-in hydrodynamical simulations (dwarfs Dwn1 and Dwn2). The CDM simulations for these systems with the aggressive refinement were also run for comparison.

[5] Although our target halos/galaxies have masses at $z \sim 0$ much larger than the scale where fake structures would form (see Fig. 1), the artificial fragments could affect our results at very high redshifts.

[6] We use a variant of the bound density maxima (BDM) halo finder algorithm of Klypin et al. (1999), kindly provided by A. Kravtsov, and run it on the dark matter particles in order to identify the dark matter halos or subhalos. The central galaxy is then centered at the position of the corresponding most massive halo.

TABLE 1
PHYSICAL PROPERTIES OF WDM RUNS AT Z = 0

Name	$\log(M_{\rm v})$ ($M_\odot$)	$\log(M_s)$[a] ($M_\odot$)	$\log(M_g)$ ($M_\odot$)	$V_{\rm max}$ (km s^{-1})	R_e[b] (kpc)	$R_{\rm v}$ (kpc)	f_g[c]	$M_{g,cold}/M_g$[d]	D/T[e]	$z_{f,h}$[f]	T[g] (Gyr)
$m_p = 0.0$ keV (CDM)											
Dw3	10.46	8.73	8.07	56.07	1.02	78.50	0.18	0.81	0.01	2.30	9.67
Dw4	10.38	8.38	8.61	52.87	0.80	73.64	0.63	0.67	0.19	1.90	8.90
Dw5	10.46	8.55	9.08	61.52	1.10	77.34	0.77	0.82	0.49	1.90	8.79
Dw7	10.39	8.21	8.60	43.44	2.20	73.90	0.71	0.75	0.59	1.70	6.79
Dwn1	10.63	8.90	9.23	63.71	2.83	89.77	0.68	0.91	0.66	2.10	6.84
Dwn2	10.58	8.72	9.13	62.73	1.25	84.20	0.72	0.86	0.57	1.50	9.45
$m_p = 1.2$ keV ($\rm WDM_{1.2}$)											
Dw3	10.43	8.74	8.92	47.87	2.03	75.24	0.60	0.86	0.43	1.85	4.89
Dw5	10.29	7.80	8.28	37.57	1.51	68.86	0.76	0.56	0.46	1.86	6.42
Dwn1	10.47	8.43	8.29	43.23	3.61	78.79	0.42	0.42	0.65	1.85	5.48
Dwn2	10.45	8.41	9.00	49.34	3.85	76.60	0.80	0.80	0.73	1.50	6.26
$m_p = 3.0$ keV ($\rm WDM_{3.0}$)											
Dw3	10.36	8.67	6.27	50.83	0.86	72.54	0.004	0.00	0.00	2.60	9.69
Dw4	10.35	8.21	7.75	48.07	0.80	72.50	0.26	0.20	0.14	2.10	10.09
Dw5	10.44	8.47	9.07	58.23	1.44	76.23	0.80	0.87	0.55	2.10	7.95
Dw7	10.38	7.99	8.73	42.80	3.08	73.23	0.85	0.60	0.78	1.60	5.69

[a]Mass within $0.1R_{\rm v}$(the same applies for M_g);
[b]Radius that encloses half of the stellar mass within $0.1R_{\rm v}$;
[c]$f_g \equiv M_g/(M_g + M_s)$;
[d]The amount of cold gas inside the galaxy in units of M_g
[e]Ratio of the mass contained in the high-angular momentum disk stars with respect to the total stellar mass;
[f]Redshift at which the given halo acquired one third of its present-day mass.
[g]Stellar mass-weighted average age.

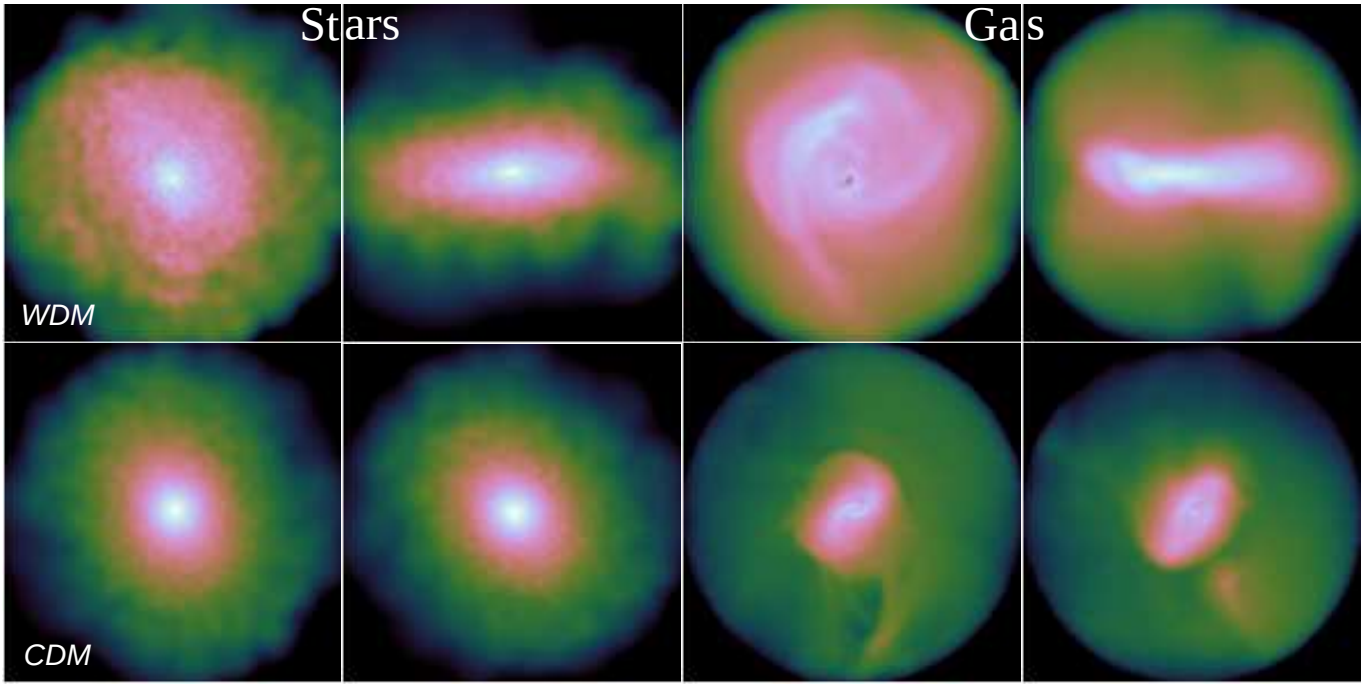

FIG. 2.— Stellar (two leftmost panels) and gas (two rightmost panels) projected distributions at $z = 0$ for the dwarf Dw3 in the $\rm WDM_{1.2}$ (top) and CDM (bottom) runs within a sphere of radius 0.15 $R_{\rm v}$. The first and third (second and fourth) columns are projections in the face-on (edge-on) planes of the galaxy. The $\rm WDM_{1.2}$ run clearly show a more extended gaseous and stellar structure than its CDM counterpart.

In Table 1, we present all the runs studied in this paper and summarize their main present-day properties. The WDM runs are shown in Fig. 1. As far as we are aware of, our simulations are the only ones, perform within the full N-body + hydrodynamical scheme, that focus on halo/galaxy masses that at present-day are close to the filtering scale M_f (corresponding specifically to $m_{\rm WDM}$=1.2 keV). The galaxy properties (M_s, stellar galaxy half-mass radius R_e, SFR, etc.) are computed within a sphere of $0.1R_{\rm v}$ radius. We notice that the $R_e$values reported in Table 1 of G+2014 were erroneously boosted by a factor $1/h$; the values presented in Table 1 here are the correct ones. This radius 0.1 $R_{\rm v}$ contains essentially all the stars and cold gas of the simulated central galaxy. The contamination of satellites or other substructures at this radius is negligible. On the other hand, because the outer stellar mass density profiles decrease strongly with radius in most of the runs, the galaxy stellar mass would not differ significantly had we measure it at "aperture" radii slightly smaller than $0.1R_{\rm v}$ by, for example, 20-50%. The disk-to-total ratio (D/T) is found using a kinematic decomposition of the stellar galaxy into an spheroid and a disk. The mass of the spheroid, M_{sph}, is defined as two times the mass of the stellar particles inside $0.1R_{\rm v}$ that have negative spin values (counter-rotate), it implicitly assumes that the spin distribution of the spheroid is symmetric around zero. The D/T is then defined as $(M_s - M_{sph})/M_s$.

4. RESULTS

4.1. *General properties*

All of our zoom-in simulations are for *distinct* halos that at the present epoch end up with virial masses of $\approx 1.5 - 3 \times 10^{10}\ h^{-1}{\rm M}_\odot$; the dwarf galaxies inside these halos are therefore *centrals*. Those halos of masses around M_f (runs $\rm WDM_{1.2}$) are devoid of substructures and have mass distributions less concentrated than their CDM and $\rm WDM_{3.0}$ counterparts. In Fig. 2, we plot the 2D stellar and gaseous distributions at $z = 0$ for dwarf Dw3 in the $\rm WDM_{1.2}$ (top) and CDM (bottom) runs. Projections in the face-on (first and third columns) and edge-on (second and fourth columns) planes of the galaxy are shown. The FITS images of these projections were obtained with TIPSY[7]. In these images, the galaxy disk lies on the plane perpendicular to the angular momentum vector of the gas cells that are within a sphere of radius $0.15R_{\rm v}$, centered on the center of mass of the stellar particles. We use then the DS9 visualization program[8] to create the images by color coding the density of the respective components within a fixed range of values for a fair comparison between the panels.

From a visual inspection of Fig. 2, we see that the $\rm WDM_{1.2}$ dwarf galaxy has a more extended and less centrally concentrated stellar mass distribution than in the CDM case. Indeed, the R_e of the former is 2 times larger than the one of the latter (see Table 1). Moreover, the former has a more disk-like structure than the latter. Indeed, we measure a disk-to-total mass ratio, D/T, of 0.43 vs 0.01 (Table 1). A more pronounced disk-like structure for the former than for the latter is also seen in the gas distribution. The $\rm WDM_{1.2}$ dwarf at the half-mode mass is gas rich (f_g=0.60) and it has an extended and a low-surface density gaseous disk, unlike the CDM case, where the dwarf is gas poor (f_g=0.18) and has a compact gas distribution. The spatial temperature distribution of the gas is also quite different: in the CDM case the gas in the galaxy is colder than the one in the dwarf at the half-mode mass scale, while the gas in the corona is hotter.

According to Table 1, the present-day dwarfs Dw3, Dw5, Dwn1 and Dwn2, formed in halos of masses around M_f, are systematically more extended (larger R_e), have a lower stellar mass and maximum circular velocities, $V_{\rm max}$, and, in most of cases, end up with a higher gas fractions than their CDM counterparts. These differences are likely a consequence of *the later assembly, lower concentrations and absence of mergers of the halos at the filtering mass*. However, due to the complex and non-linear subgrid physics, small variations in the non-linear evolutionary processes can also produce large differences and shifts in the galaxy properties at any given epoch. This is why we have simulated several systems to verify that the differences between the $\rm WDM_{1.2}$ dwarfs and their CDM counterparts are systematical and not due to small variations in a particular case. Moreover, although the systems with masses much larger than M_f (runs $\rm WDM_{3.0}$) show some differences with respect to their CDM counterparts, these are already small and do not follow a systematical trend as in the case of the $\rm WDM_{1.2}$ runs. For example, in some $\rm WDM_{3.0}$ runs f_g, R_e or D/T are larger in the $\rm WDM_{3.0}$ runs than in their CDM counterparts, while in others they are smaller. This very likely means that the differences are due to small variations in the non-linear evolution rather than due to the (small) differences in the initial power spectrum. Yet, $V_{\rm max}$ is systematically lower in all $\rm WDM_{3.0}$ runs, but not by much as seen in the case of the $\rm WDM_{1.2}$ ones. *The depth of the gravitational potential of the systems seems to be the main property systematically affected by the filtering in the power spectrum of fluctuations.*

4.1.1. *Radial distributions*

In this subsection, we explore in more detail the present-day inner structure and dynamics of the simulated dwarfs. Solid lines in Fig. 3 show the total circular velocity profiles, $V_c(r)$, and their decompositions into DM, stars and gas (gray, blue and cyan lines, respectively) for the systems of mass around M_f (runs $\rm WDM_{1.2}$, upper panels) and of mass $(20 - 30) \times M_f$ (runs $\rm WDM_{3.0}$, lower panels). The corresponding CDM dwarfs are also shown with dashed lines using the same color coding. The total circular velocity profiles (magenta lines) for dwarfs formed in halos at the filtering scale are *shallower in the center than the CDM counterparts with lower values of* $V_{\rm max}$ *by* 20-60%. These differences can be seen even for dwarfs formed in the $\rm WDM_{3.0}$ cosmogony, though they are small, showing that systems formed in halos much larger than M_f tend to be similar to those formed in the CDM scenario.

The stellar $V_c(r)$ components (blue lines) of the $\rm WDM_{1.2}$ runs are significantly lower and less peaked than the CDM cases. In all simulations, the halo component dominates, at least from radii larger than $\sim 0.1 - 0.7\ R_e$. The circular velocities of the gaseous component (cyan lines) tend also to be less peaked in the $\rm WDM_{1.2}$ runs

[7] http://www-hpcc.astro.washington.edu/tools/tipsy/tipsy.html
[8] http://ds9.si.edu/site/Home.html

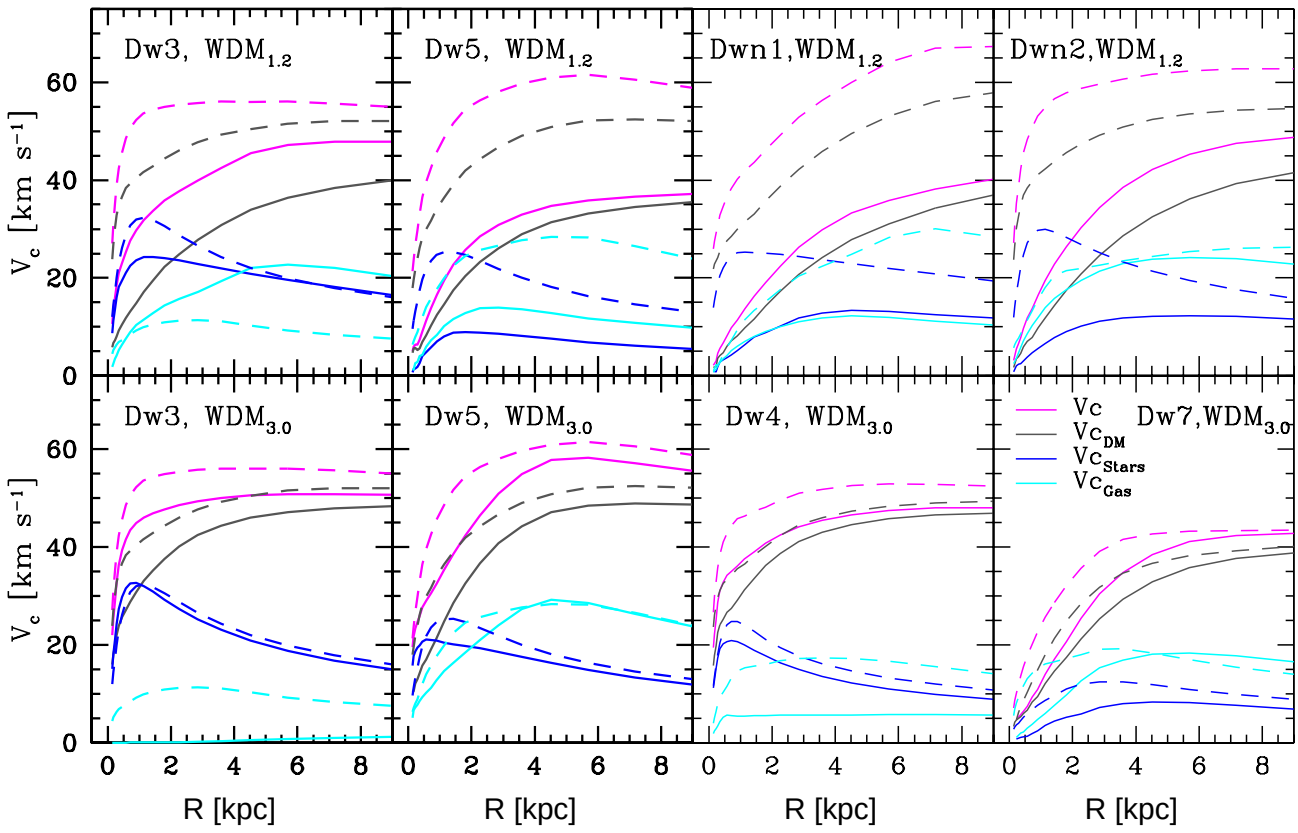

FIG. 3.— Circular velocity profiles and their decomposition for the WDM runs (solid lines) and their CDM counterparts (dashed lines) at $z = 0$. In the upper panels are plotted the profiles for the systems of masses around the filtering scale M_f and in the lower panels for those systems of masses 20 to 30 times M_f. We denote with magenta, gray, blue, and cyan lines the total, halo, stellar, and gaseous circular velocities, respectively.

than in the CDM ones. However, while in the CDM case their inner contributions to the total circular velocity lie below that of the stellar component, except for dwarf Dw7, in the case of the $WDM_{1.2}$ runs, the $V_c(r)$ of the gaseous component is similar or dominates at all radii over the stellar one, except in the inner region of dwarf Dw3 ($WDM_{1.2}$ dwarfs are more gaseous than the analogous CDM dwarfs, see Table 1). In any case, the baryonic (stellar + gaseous) contribution to the total $V_c(r)$ is more important and *more centrally concentrated* in all CDM runs than in the $WDM_{1.2}$ ones. Therefore, the circular velocities of the WDM systems of masses around M_f are shallower than the CDM ones mainly because *less centrally concentrated baryonic galaxies form in the former simulations* (see also Fig. 4 below).

On the other hand, $V_{\rm max}$ is significantly lower in the $WDM_{1.2}$ runs than in the CDM ones mainly because the corresponding pure DM halos are already less concentrated in the WDM case than in the CDM one (e.g, Avila-Reese et al. 2001; Lovell et al. 2012). However, the astrophysical processes in both cases are also expected to produce different effects on the inner dynamics of the galaxy-halo systems, which could increase/reduce the differences in $V_{\rm max}$, as well as in the innermost dynamics of the galaxy-halo systems (for instance, the formation or not of shallow cores). We will study in detail this question elsewhere.

In Fig. 4, the stellar (blue) and cold gas (cyan) surface density (SD) profiles of the $WDM_{1.2}$ and $WDM_{3.0}$ runs (solid lines) are compared to those of their CDM counterparts (dashed lines). The most noticeable difference in the stellar SD profiles between the $WDM_{1.2}$ runs and the corresponding CDM ones (upper panels) is that *the inner regions of the former are significantly lower*. While the CDM dwarfs have a central peaked stellar density, reminiscent of a bulge-like structure, in the $WDM_{1.2}$ ones a flattened SD is seen, except in run Dw3; though, even in this case, the CDM dwarf has a more peaked SD (see also Fig. 3). Regarding the gas SD profiles, for the CDM dwarfs, they tend to be more extended than the stellar ones and of lower SDs in the center, while for the $WDM_{1.2}$ dwarfs, the gas SD profiles roughly follow the stellar ones, except for run Dw3. The CDM dwarfs have higher baryonic (stars+gas) SDs in the center than the dwarfs formed in halos at the filtering scale. In the case of the $WDM_{3.0}$ dwarfs (lower panels), their stellar and gas SD profiles tend to be similar to those of their CDM counterparts; though, for Dw4 and Dw7 the gas SD profiles show significant differences.

The systematical differences in the stellar SD profiles between the $WDM_{1.2}$ and CDM runs, specially in the inner regions, could be the result of many effects. One of them might be the angular momentum of the halos in which galaxies form. We have measured the halo (dark matter particles only) spin parameter[9] λ for all the runs

[9] The spin parameter is defined as $\lambda = \frac{J|E|^{1/2}}{GM^{5/2}}$, where J, M

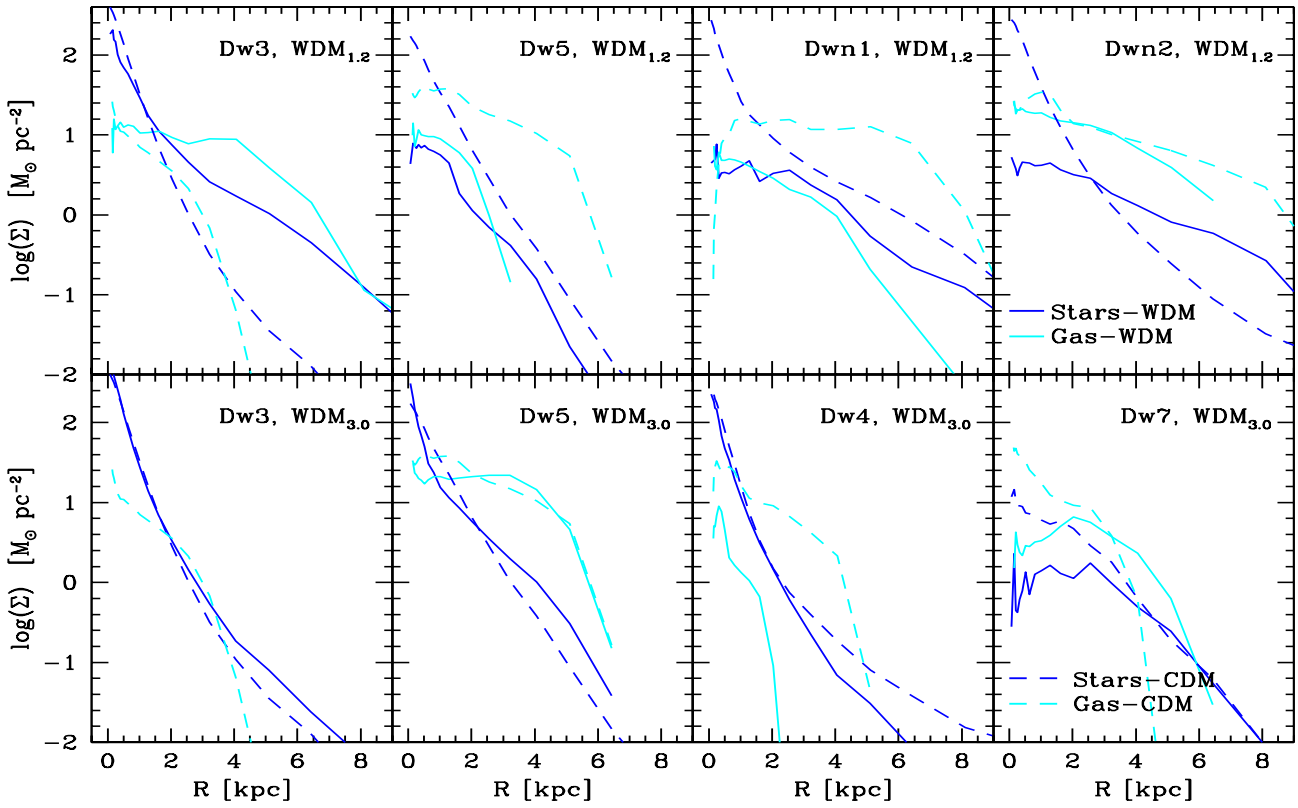

FIG. 4.— Stellar (blue lines) and gas (cyan lines) surface density profiles of the WDM dwarfs (solid lines), compared to their CDM counterparts (dashed lines). The upper and lower panels are for the $WDM_{1.2}$ and $WDM_{3.0}$ runs, respectively.

at $z = 0$ with the following results: runs Dw3 and Dw5 have a lower spin parameter in the CDM runs than in the $WDM_{1.2}$ ones (0.015 and 0.007 vs. 0.033 and 0.012, respectively) but for runs Dwn1 and Dwn2 we found the contrary, CDM runs have a higher spin parameter (0.072 and 0.083 versus 0.032 and 0.037, respectively). The last two runs, specially Dwn2, have a relatively late merger in the CDM simulations that could affect the spin parameter, although these mergers happened more than ~ 4 Gyr ago. We have also measured the spin parameter by using the alternative definition of λ introduced in Bullock et al. (2001). Although the values of λ are different, the trend is the same: runs Dwn1 and Dwn2 have larger values in the CDM simulations, and Dw3 and Dw5 have smaller values. In summary, it is not clear that the halo spin parameter is the reason why the stellar distribution is less concentrated in the WDM runs than in the CDM ones. We plan to study in detail elsewhere (Avila-Reese et al in prep) the question of the spin parameter in WDM and CDM, both in DM-only and hydrodynamical simulations.

The mechanism responsible for the stellar-SD profile differences between the $WDM_{1.2}$ and CDM dwarfs can be traced probably to the merging history of the central galaxies (Herpich et al. 2014). The satellite interactions/mergers in the case of CDM simulations drive gas to the center, where SF proceeds efficiently, producing a cuspy stellar structure. The stellar specific angular momentum is also more likely to decrease in the galaxies that suffered mergers since the angular momentum of these merging galaxies can cancel each other (Cloet-Osselaer et al. 2014). These processes do not happen in the $WDM_{1.2}$ dwarfs because they are practically devoid of satellites. Besides, the galaxy assembly starts later than in the CDM halos, being the disks more gaseous and less susceptible to secular evolutionary processes.

In summary, dwarfs formed in halos of masses around M_f in our $WDM_{1.2}$ simulations have a quite different dynamical history and structural inner properties when compared to their CDM counterparts, whereas dwarfs formed in a WDM cosmology but in halos with a mass much larger than M_f, tend to be similar to the corresponding CDM dwarfs. The latter is in agreement with the simulation results of Herpich et al. (2014).

4.2. *Mass assembly histories*

In Fig. 5 we plot the virial MAHs of the $WDM_{1.2}$ (upper panels) and $WDM_{3.0}$ (lower panels) runs along with their corresponding CDM counterparts (black solid and dashed lines, respectively). As can be seen, the halos around the filtering mass M_f start to assemble later and end up with masses slightly smaller than the corresponding CDM ones. However, afterwards the former grow faster, specially the runs Dw3 and Dw5. Thus, the epoch at which half or one-third of the present-day virial mass is acquired is not very different between both cosmologies (see Table 1). The WDM halos of scales $(20 - 30) \times M_f$ assemble their masses practically in the

and E are the total angular mometum, mass, and energy, respectively. This latter quantity is computed, assuming that the halo is virialized, as -K, where K is the kinetic energy.

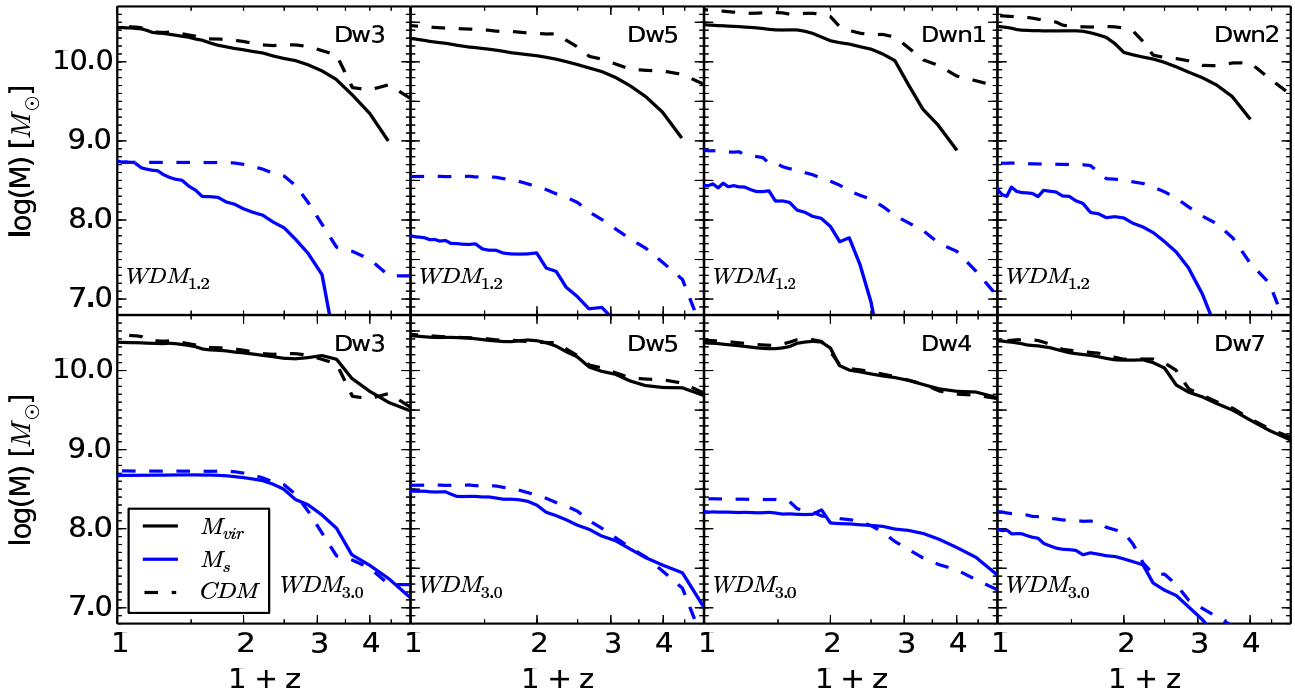

FIG. 5.— Mass assembly histories for the simulated dwarf galaxies. In the upper panels we show the MAHs for the $WDM_{1.2}$ runs, while in the lower panels are the MAHs of the $WDM_{3.0}$ runs (solid lines). In each case, the MAHs of the corresponding CDM runs are also plotted (dashed lines). We denote with black lines the total (virial) MAHs and with blue lines the galaxy stellar MAHs. The MAHs of the dwarfs formed in halos around M_f ($WDM_{1.2}$ runs) differ significantly from their CDM counterparts.

same way as they do in the CDM scenario.

The blue solid and dashed lines in Fig. 5 show the stellar MAHs of the WDM and CDM simulated dwarf galaxies, respectively. In G+2014, it was shown that the stellar MAHs of dwarfs follow roughly their halo MAHs in the CDM simulations; i.e., the M_s-to-M_v ratio is roughly constant, at least up to $z \sim 2$ (with variations of $0.1-0.4$ dex). Here, for the $WDM_{1.2}$ dwarfs we find that from $z \gtrsim 2$ to ~ 1 the M_s-to-M_v ratio significantly increases; from $z \sim 1$ to 0, this ratio continues increasing (except in run Dw5) but only slightly. The early fast increase occurs because at earlier epochs the $WDM_{1.2}$ baryonic galaxies are in their active growth phase. Thus, the stellar mass assembly of the dwarfs at the filtering scale shows a decoupling from the assembly of their halos, unlike what happens with the dwarfs in the CDM case. At $z = 0$, the M_s-to-M_v ratios of all $WDM_{1.2}$ galaxies are $2-4$ times lower than their CDM counterparts except for Dw3 in which case they are similar. As expected, the differences are much smaller when compared to the $WDM_{3.0}$ runs; at $z = 0$, the maximum difference, which amounts a factor of 1.6, is found for the dwarf Dw7. In general, the M_s-to-M_v ratio remains close to the CDM one at all redshifts. Thus, as the halo mass gets closer to the filtering mass, the galaxies formed inside them end up with lower M_s-to-M_v ratios. This result strictly holds for the scales and neutrino masses (1.2 and 3.0 keV) studied here.

Our $WDM_{1.2}$ dwarf galaxies assemble their stellar masses with a significant delay with respect to their CDM counterparts. For example, the assembly of half of the present-day M_s for dwarf Dw5 happens 1.3 Gyr later in the $WDM_{1.2}$ cosmology. For the dwarfs formed in halos much larger than M_f (runs $WDM_{3.0}$), the stellar MAHs are close to those of the CDM counterparts, with minimum differences in the half-mass assembly epochs.

The galaxy baryon (stars + gas) MAHs, $M_b(z)$, of the simulated galaxies follow moderately the halo MAHs, with some intermittence, both in the WDM and CDM simulations. However, the $WDM_{1.2}$ runs show more intermittent histories than the CDM ones, due to more extended periods of gas infall/outflow onto/from the halos. This is likely because the $WDM_{1.2}$ halos accrete baryons in a more regular way than the CDM halos and because they blowout the gas more efficiently due their lower concentrations and V_{max}. The baryon-to-halo mass ratios, M_b-to-M_v, of the former are slightly lower than those of the latter at all epochs, except for run Dw3 at $z \lesssim 0.7$. In particular, at $z = 0$, the M_b-to-M_v ratios of the $WDM_{1.2}$ galaxies are $1.1-3.5$ times lower than their CDM counterparts.

4.3. *Gas fraction and star formation histories*

In Fig. 6, we plot the change with redshift of the *galaxy* gas fractions (f_g=M_g/M_b, solid lines) for the $WDM_{1.2}$ and $WDM_{3.0}$ runs, upper and lower panels, respectively. The dashed lines show the change with redshift of the fraction of gas outside the galaxy but within the *halo*, the"halo" gas fraction $F_{g,h}$. This is defined as the ratio of the gas mass contained in the spherical shell of radii between $0.1R_v$ and R_v to the gas mass in the whole halo. As in the case of the CDM simulations (see Fig. 6 in G+2014), the two gas fractions oscillate, and in periods

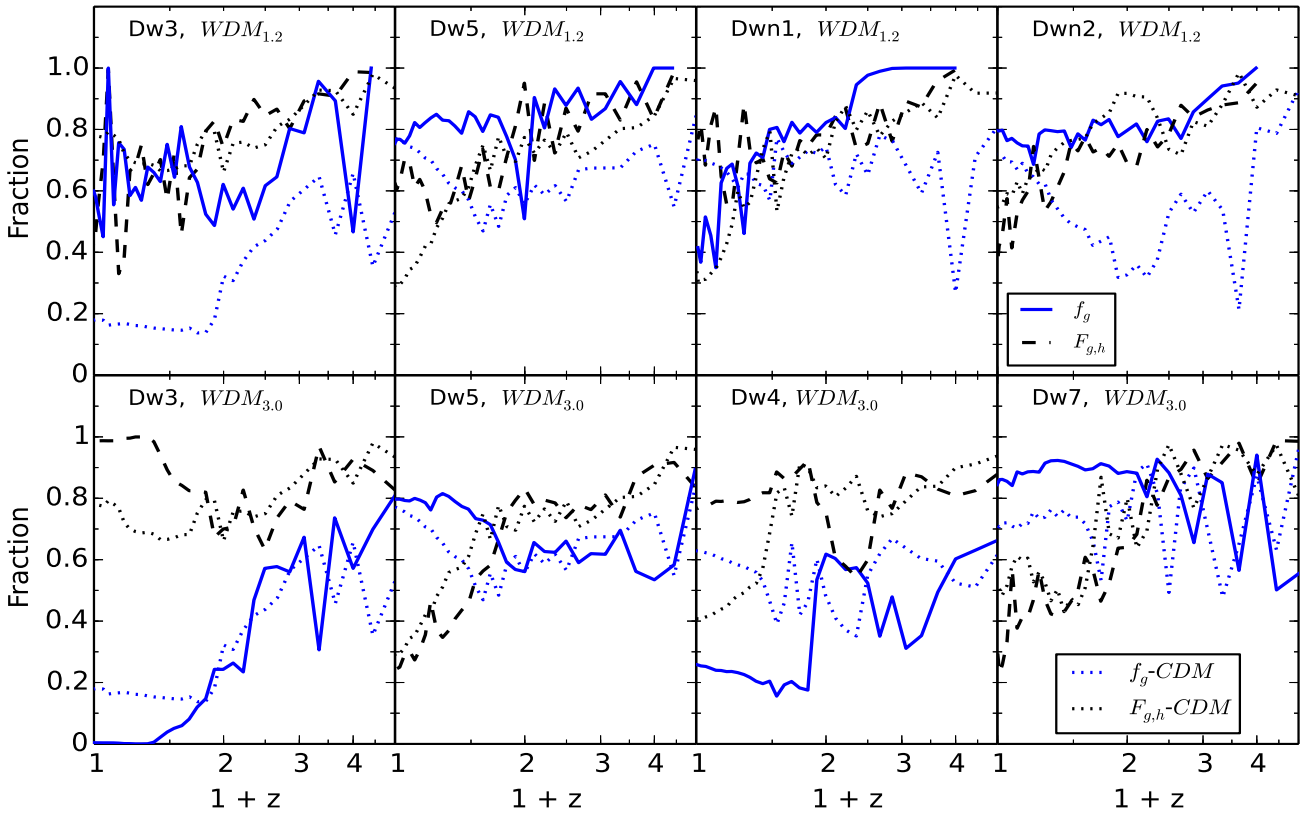

FIG. 6.— Evolution of the galaxy gas mass fraction, f_g, for the different WDM runs (blue solid lines). The black dashed line refers to $F_{g,h}$, the ratio between the gas mass in the halo (the gas in the spherical shell of radii $0.1R_{\rm v}$ and $1R_{\rm v}$) and the total gas mass within $R_{\rm v}$. With blue and black dotted lines, f_g and $F_{g,h}$, respectively, we show the corresponding quantities for the CDM case. The $\rm WDM_{1.2}$ runs, plotted in the upper panels, present evolutions of f_g and $F_{g,h}$ that differ significantly from those of their CDM counterparts, while, on ther other hand, for the $\rm WDM_{3.0}$ runs, plotted in the lower panels, the differences are less notorious.

where f_g decreases (increases) typically $F_{g,h}$ increases (decreases). This is mainly due to the interplay among gas accretion onto the galaxy, SF and SN-driven outflows from the galaxy. It seems that this interplay is stronger in the CDM simulations than in the systems with mass around M_f ($\rm WDM_{1.2}$). The $\rm WDM_{3.0}$ runs show a behavior roughly close to their CDM counterparts.

The galaxy gas fractions in the $\rm WDM_{1.2}$ runs are, at all epochs, higher than those found in their CDM runs counterparts, probably as a consequence of the later galaxy assembly of the former runs. The values of f_g at $z = 0$ are shown in column eighth of Table 1. We see that the f_g values of the WDM dwarfs formed in halos of scales around M_f are relatively high.

In Fig. 7 we plot the "archeological" SF histories of our WDM runs (solid lines) compared to their CDM counterparts (blue dashed lines). For illustration purposes, since the SF histories are strongly intermittent, they were smoothed with a top-hat filter of 500 Myr width. The original histories were built with 0.1 Gyr bins. This is computed, for any given time t [Gyr], identifying all galaxy stellar particles at $z = 0$ born within the time interval $[t-0.1,t]$ Gyr; the SFR at this time is then simply the mass of these particles divided by 0.1 Gyr.

As expected from the later halo assembly, the SF in the $\rm WDM_{1.2}$ systems of masses around M_f starts later than in the CDM counterparts. Besides, the former present *more sustained SF histories at later epochs than the CDM dwarfs*, for which the SFR tends to fall in the last Gyrs. This implies that the specific SFRs ($\rm SFR/M_s$) of the WDM galaxies of scales around M_f tend to be higher at late epochs than those of the CDM counterparts. The fact that the $\rm WDM_{1.2}$ galaxies assemble later and have lower central gas surface densities than the CDM ones likely explains their less efficient but more sustained SF histories. As in the CDM runs (see a discussion in G+2014), the SF histories in the WDM runs are also episodic. For those systems around the filtering mass M_f, the SF is sometimes even more bursty than their CDM counterparts.

To highlight the differences in the stellar populations between the dwarfs in the $\rm WDM_{1.2}$ runs and their CDM counterparts, in Fig. 8 we plot the cumulative (archaeological) SF histories. Solid lines are for the $\rm WDM_{1.2}$ and $\rm WDM_{3.0}$ dwarfs, left and right panel, respectively, while dashed lines in both panels are for the CDM counterparts. One clearly sees that the stellar populations of present-day $\rm WDM_{1.2}$ dwarfs are formed on average significantly later than those of the CDM dwarfs, with 20% of their stars being formed in the last ~ 4 Gyr; in contrast, the CDM dwarfs, have formed already 80% of their stars between ~ 7.5 and 9 Gyr ago (Dwn1 reaches this fraction later, ~ 4.6 Gyr ago). The galaxy Dw3 is the one that most differs in its SF history (black lines), when compared $\rm WDM_{1.2}$ with CDM, and Dwn1 is the one that shows the most similar history (blue lines). Interestingly, it is the galaxy Dw3 the one that differs less when compared $\rm WDM_{3.0}$ with CDM. In general, the dif-

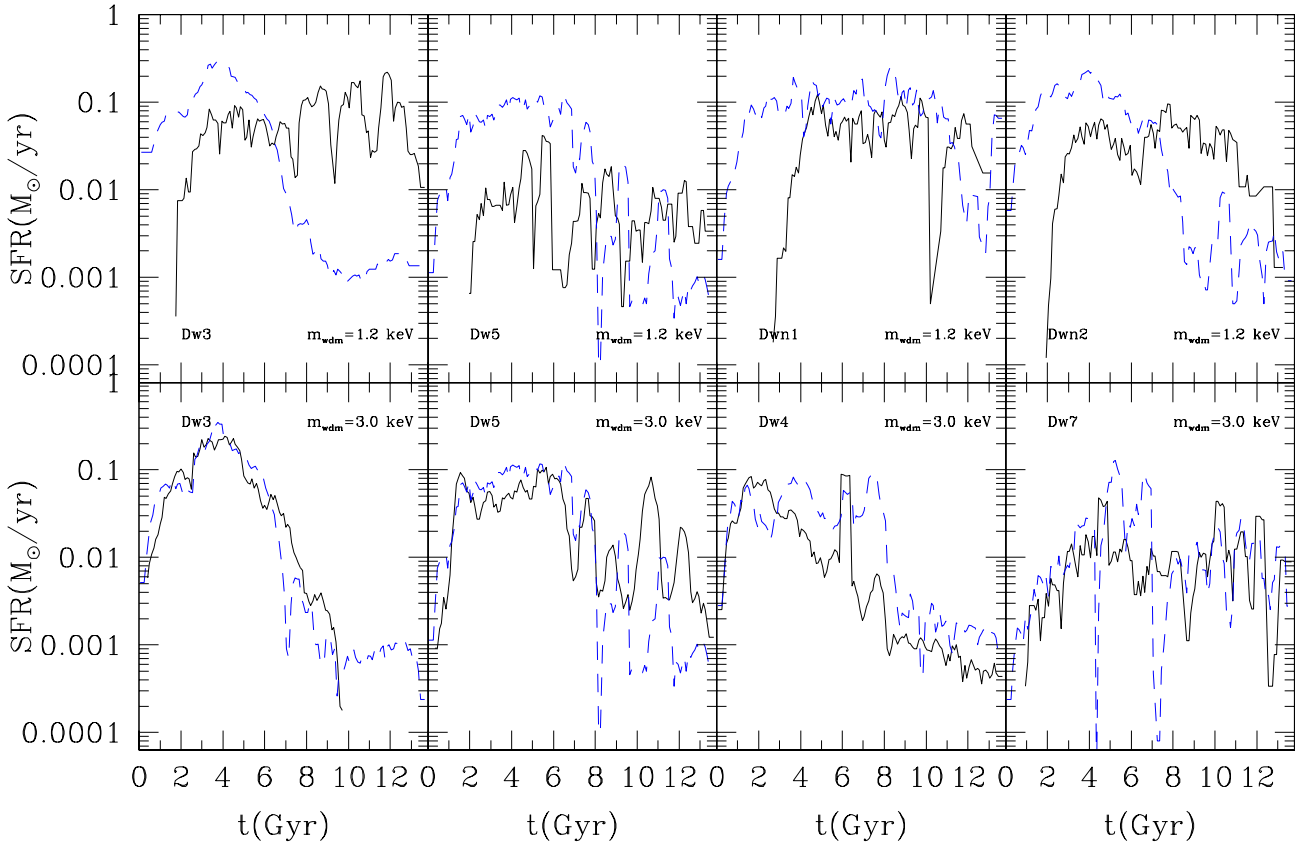

FIG. 7.— Archaeological SF rate histories for the $WDM_{1.2}$ (upper panels) and $WDM_{3.0}$ (lower panels) runs presented in this paper (black solid lines). In each panel, the corresponding CDM SF histories are also shown (dashed blue lines). In the x-axis runs the cosmic time. The histories were smoothed with a top-hat filter of 500 Myr width; see text for details about how the SF histories were calculated.

ferences between the $WDM_{3.0}$ and CDM galaxies (right panel), as expected, are lower than those found when the $WDM_{3.0}$ and CDM dwarfs are compared.

We have calculated also the mass-weighted "archeological" ages of all runs and report them in the last column of Table 1. This age is the result of multiplying the age of each galaxy stellar particle at $z = 0$ by its mass fraction contribution (the particle mass divided by M_s), and summing these terms for all the particles. *The dwarfs of scales around M_f are between $\sim$ 1.4 and 4.8 Gyrs younger than their CDM counterparts.* The largest difference is for the dwarf Dw3 and the smallest for Dwn1 (see above). The mass-weighted ages of the $WDM_{3.0}$ dwarfs are similar or slightly smaller (by $\sim$ 1 Gyr) than the CDM counterparts. In summary, *central dwarf galaxies in the WDM scenario are expected to have younger stellar populations on average than their CDM counterparts,* the younger the closer their halo masses are to the filtering scale.

5. SUMMARY AND DISCUSSION

We have presented the first N-body + Hydrodynamics (zoom-in) simulations of galaxies formed in distinct WDM halos with masses at present-day close to the half-mode filtered mass M_f corresponding to a thermal WDM particle mass of $m_{\rm WDM}$=1.2 keV. Halo masses are around 3×10^{10} $M_\odot$. Galaxies formed in WDM halos 20–30 times more massive than M_f were also simulated (runs $WDM_{3.0}$, for which $m_{\rm WDM}$=3.0 keV). In a WDM cosmology, the halos of masses around M_f are close to the peak of the halo mass function; at masses a factor of $\sim 2-3$ lower, the halo mass function declines sharply due to the damping of the initial power spectrum of fluctuations (e.g., Schneider et al. 2013; Angulo et al. 2013). Most of structures $\sim$ 3 times smaller than M_f at $z = 0$ already do not appear to be virialized spherical overdensities (halos) and they did not assemble hierarchically.

Our results show that the $WDM_{1.2}$ galaxies have disk-like structures and circular velocity profiles that gently increase and then flattens. These dwarfs are quite different in several aspects from their CDM counterparts, which assembled hierarchically. The galaxies formed in halos $20-30$ times M_f (runs $WDM_{3.0}$), instead, are very similar in properties and evolution to their CDM counterparts, in agreement with the results of Herpich et al. (2014). Therefore, *the properties and evolution of WDM galaxies differ more from those of the CDM galaxies as the mass get closer to the filtering scale.* In summary, our $WDM_{1.2}$ dwarf galaxies that formed in halos with a mass around M_f differ from their CDM counterparts in that:

1. they assemble their stellar masses later (Fig. 5), with archaeological SF histories shifted to younger stellar populations (Fig. 8; on average, the WDM dwarfs have mass-weighted ages 1.4–

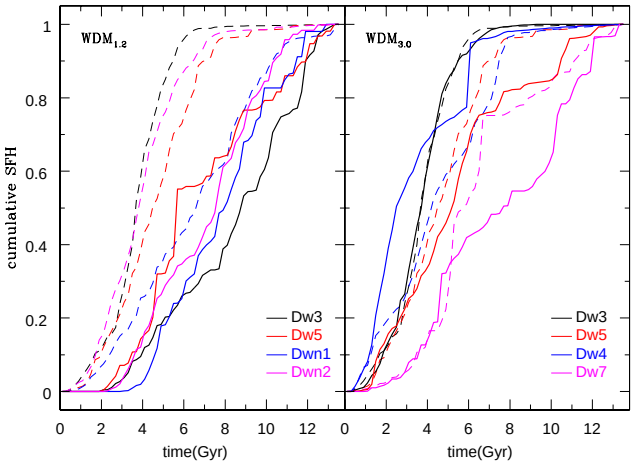

FIG. 8.— Cumulative SF histories of the $WDM_{1.2}$ and $WDM_{3.0}$ runs (solid lines), left and right panel, respectively, along with their CDM counterparts (dashed lines in both panels). The different dwarfs are identified with different colors. The $WDM_{1.2}$ runs clearly form most of their present-day stars much later than their CDM counterparts. As expected, the differences between the $WDM_{3.0}$ and CDM runs (right panel) are lower than those found in the left panel, although there are runs and periods in which these differences are significant.

4.8 Gyr younger than the CDM ones, see also Governato et al. 2014);

2. their $V_{\rm max}$ values are 20–60% lower;

3. they have significantly lower central stellar SDs and larger R_e values, by factors of 1.3–3 (Fig. 4);

4. their $V_c(r)$ profiles are shallower, being this mainly because the baryonic (stars + gas) components are shallower (Fig. 3);

5. on average, they have higher gas fractions and lower stellar masses (and thus lower M_s-to-$M_{\rm v}$ ratios).

As stated above, the reported differences were found in galaxies formed in halos with the particular value for the filtering scale of $M_f = 2 \times 10^{10}\ h^{-1}{\rm M}_\odot$ ($m_{\rm WDM} = 1.2$ keV). Can these results be generalized to other scales (or WDM particle masses)? We could argue that at least qualitatively our results might be extended to other masses because part of the these differences, lower Vmax, M_s-to-$M_{\rm v}$ ratios, etc., are systematically due to the lower concentrations and delay in the formation of the WDM halos. Nevertheless, in general, the results of our hydrodynamic simulations should not be rescaled with respect to the filtering mass because the astrophysical processes such as cooling, feedback, etc., affect significantly the evolution of the galaxy-halo systems, specially in small halos (higher WDM particle masses).

5.1. *WDM galaxy formation*

If the Ly-α power spectrum constrains WDM models to be made of relic particles with masses above ≈ 3 keV (Viel et al. 2013), then the corresponding filtering scale at $z = 0$ should be $\lesssim 1.5 \times 10^9$ ${\rm M}_\odot$. In the CDM cosmology, the distinct halos of 1.5×10^9 ${\rm M}_\odot$ have $V_{\rm max}$ values of ~ 20 km/s and their stellar masses are expected to be $\lesssim 10^7 - 10^6$ ${\rm M}_\odot$ (M_s-to-$M_{\rm v}$ ratios $\lesssim 7 - 0.7 \times 10^{-3}$), depending on the used subgrid physics (e.g., Sawala et al. 2010; Munshi et al. 2013; Cloet-Osselaer et al. 2014; Sawala et al. 2014a,b; Governato et al. 2014).

If we now extend our results found in this work; that is, the differences found between the $WDM_{1.2}$ and CDM simulations, to the hypothetical dwarfs formed in halos at the filtering scale of 1.5×10^9 ${\rm M}_\odot$ ($m_{\rm WDM}$=3 keV), then the corresponding $V_{\rm max}$ and $M_s/M_{\rm v}$ ratio would be around 12 km/s and 0.005, respectively. On the other hand, we would expect these WDM dwarfs to have higher gas fractions, lower central stellar SDs and later SF histories than the corresponding CDM ones. As mentioned above, the results of the hydrodynamic simulations may or may not be generealized to other filtering scales, so this extrapolation of our results should be considered just as a qualitative statement.

Unfortunately, current observations of field dwarf galaxies of masses and circular velocities as small as those corresponding to halos of masses $\sim 10^9$ ${\rm M}_\odot$ are so limited that they can not be used to distinguish between the CDM and the WDM with $m_{\rm WDM} \approx 3$ keV cosmogony. The few and uncertain observations of central (field) very small dwarfs point out that practically all of them are star-forming and gaseous rich galaxies (e.g., Geha et al. 2006, 2012), with late SF histories (e.g., Weisz et al. 2014; Cole et al. 2014), and with $V_{\rm max}$ values for a given M_s smaller than those inferred or simulated in the CDM scenario (e.g, Ferrero et al. 2012; Rodríguez-Puebla et al. 2013), thus favoring the WDM scenario. However, as several authors have shown, these potential disagreements in the CDM scenario, in particular those related to the too-high $V_{\rm max}$ and $M_s/M_{\rm v}$ values, could be solved also by plausible changes/improvements in the subgrid physics; for example, by introducing a metallicity-dependent H_2 molecule formation process (Kuhlen et al. 2012; Christensen et al. 2012) or by introducing preventive/early mechanisms of feedback besides of increasing the strength of the ejective SN-driven feedback (Hopkins et al. 2012, 2014; Munshi et al. 2013; Trujillo-Gomez et al. 2013; Stinson et al. 2013; Agertz et al. 2013).

Along this venue, Governato et al. (2014, see also a recent review by Brooks 2014)) argue that the effects of the SF-driven feedback overcome those of the initial power spectrum regarding the inner dark matter and stellar mass distributions. This conclusion is based on only one zoom-in simulated dwarf in both CDM and WDM cosmologies. For the latter, the filtering corresponds to a relic particle of mass 2 keV, which means that $M_f = 5.7 \times 10^9$ ${\rm M}_\odot$ (see Fig. 1). The present-day virial mass of their dwarf is $\approx 1.4 \times 10^{10}$ ${\rm M}_\odot$ (after correcting by a factor of 1.23 as one goes from M_{200} to $M_{\rm v}$); that is, this system is ≈ 2 times larger than the filtering mass. For this particular object, the dark-matter only simulations in the CDM and WDM cosmologies show that their $V_c(r)$ profiles are actually not too different from each other (see their Fig. 8).

At the level of dark-matter only simulations, the four $WDM_{1.2}$ halos (to be presented elsewhere, Avila-Reese et al. in preparation) show different $V_{\rm max}$ values and

$V_c(r)$ profiles as compared with the corresponding CDM halos. There are also significant differences regarding the assembly histories. Thus, the effects of the damping of the power spectrum seem to have significant effects on the structures close to M_f already in pure N-body simulations. WDM halos at the cutoff of the power spectrum are certainly different than the CDM ones and, when baryons are included in the simulations, the initial conditions could leave an imprint in the respective galaxies. Note that the astrophysical effects also affect the dark matter halo properties so that predictions based on dark-matter only results that are then compared to observations should be taken with care (for example, when comparing the WDM halo velocity function to the observed galaxy velocity function Zavala et al. 2009; Klypin et al. 2014; Papastergis et al. 2014)

Future observational studies of central (field) dwarf galaxies will be crucial for constraining the nature of dark matter. In addition to the inner dynamics, we have also found important differences between CDM and WDM dwarfs in their SF histories, stellar SD profiles (specially in the central regions), and gas fractions.

It should be said that resolution issues are likely affecting our results regarding the earliest stages ($z > 3$) of the WDM galaxy assembly, where virial masses get closer to the scale of artificial fragmentation of filaments and to the free-streaming scale. Very high-resolution simulations, including baryons, suggest that structures around the free-streaming scale are smooth and dense filaments able to capture gas that can cool efficiently and form stars (Gao & Theuns 2007; Gao et al. 2014). Thus, the smallest (earliest) baryonic structures in a WDM cosmology are expected to be filament-like; certainly, the formation of stars (the first ones) in this environment is different from that in a virialized halo (see Gao & Theuns 2007). SF may efficiently proceed in these filaments before they disappear into the more familiar halo-like structures, so that a non-negligible fraction of stars in the $z = 0$ galaxy may have formed early in these filaments. Hence, our result that the fraction of stars formed during the first 2–4 Gyr in the $\mathrm{WDM}_{1.2}$ runs is negligible (Fig. 8) could be an underestimation due to our inability to adequately resolve and follow the physics of the gas in the first smallest filaments (their masses should be of the order of the corresponding free-streaming mass, $\sim 2 \times 10^6\ h^{-1}\mathrm{M}_\odot$).

We end the discussion by asking whether our simulated dwarfs with $m_{\rm WDM}$=1.2 keV are in agreement with observations. In Avila-Reese et al. (2011) and in G+2014 we studied the properties and evolution of CDM low-mass galaxies, some of which (Dw3, Dw4, Dw5 y Dw7) were also studied here. These CDM galaxies with total masses around $1 - 5 \times 10^{10}\ h^{-1}\mathrm{M}_\odot$ are relatively realistic in structural and dynamical properties; however, they have lower specific SF rates, too high M_s-to-$M_{\rm v}$ ratios and lower gas fractions than the observed ones, showing that they form most of their stars too early. The $\mathrm{WDM}_{1.2}$ dwarfs simulated here *with the same subgrid physics* have delayed SF histories, form less stars, and have more gas than their CDM counterparts. However, when compared to observed galaxies of similar stellar masses, they are too extended. In any case, a WDM model with $m_{\rm WDM}$=1.2 keV seems to be in conflict with the last Ly-α forest constraints (Viel et al. 2013).

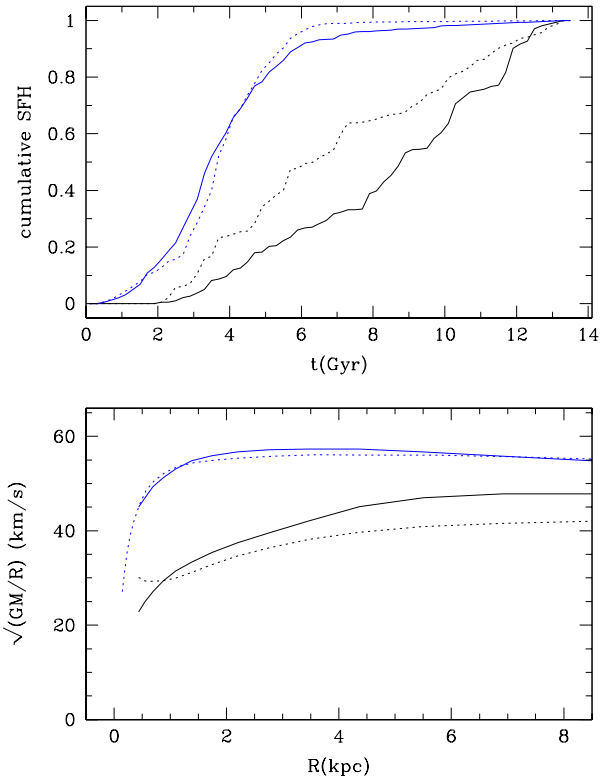

FIG. 9.— A comparison of the CDM and $\mathrm{WDM}_{1.2}$ runs, blue and black lines, respectively, of dwarf Dw3 with aggressive (dotted lines) and soft (solid lines) refinements is presented. In the upper panel we show the comparison regarding the cumulative SF history while in the lower panel the comparison is with respect to the circular velocity (see discussion in the appendix).

ACKNOWLEDGEMENTS

We are grateful to the Referee for his/her constructive comments. VA and AG acknowledge CONACyT grant (Ciencia Básica) 167332. AG acknowledges a PhD fellowship provided by DGEP-UNAM

APPENDIX

As mentioned in Section 3.1, the CDM dwarfs were run with the same refinement setting used in G+2014. However, to try to reduce the probable appearance and growth of spurious fragments, a less aggressive refinement was used in the WDM runs. This means that WDM dwarfs are slightly less resolved than their CDM counterparts; that is, the halo/galaxy ends up with less resolution elements. To show that no significant differences appear when this setting (resolution) is used, we run some of our CDM simulations with this soft refinement. In Fig. 9, we compare the cumulative SFH (upper panel) and circular velocity (lower panel) of the CDM run of Dw3 using the aggressive refinement (blue dotted lines) with the corresponding quantities of the less aggressive setting (blue solid lines). The difference between the two runs in $V_{\rm max}$ amounts only to $\sim 2\%$, while in the cumulative SFH the major differences are seen during the stage of active star formation, in the first ~ 5 Gyr. On the other hand, the late star formation seems to be somewhat sensitive to the details of the used resolution.

Yet, we certainly believe this should not be much of concern because the amount of mass in stars formed in this relatively quiet star forming phase is small; in general, the stellar mass M_s in the less resolved run is only 17% higher than the corresponding one with the aggressive refinement setting.

In Fig. 9, we also plot the $WDM_{1.2}$ runs for the same Dw3 galaxy. The use of an aggressive refinement (black dotted lines), produces older stellar populations than in the less aggressive refinement employed in the paper (black solid lines). The refinement setting clearly affects more the $WDM_{1.2}$ run than the CDM one. This is very likely related to the greater number of spurious fragments form at early times in the more aggressive setting, which are incorporated later to the halo/galaxy. The differences found in the V_c profile are also greater in the refinement setting in the $WDM_{1.2}$ run than in the CDM one. In particular, we see that the $WDM_{1.2}$ simulation with the more aggressive refinement (black dotted line) forms a centrally mass concentration (inner peak) composed of mass in stars and dark matter. This is consistent with the higher early SFR seen in the top panel. In any case, the differences in the SF history and V_c profile between the $WDM_{1.2}$ and CDM Dw3 run *remain* qualitatively the same in our simulations regardless of the refinement setting.

REFERENCES

Abazajian, K., Fuller, G. M., & Patel, M. 2001, Phys. Rev. D, 64, 023501
Agertz, O., Kravtsov, A. V., Leitner, S. N., & Gnedin, N. Y. 2013, ApJ, 770, 25
Anderhalden, D., Schneider, A., Macciò, A. V., Diemand, J., & Bertone, G. 2013, JCAP, 3, 14
Angulo, R.E., Hahn, O., & Abel, T. 2013, MNRAS, 434, 3337
Avila-Reese, V. Colín, P., Valenzuela, O., D'Onghia, E., & Firmani, C. 2001, ApJ, 559, 516
Avila-Reese, V., Colín, P., Piccinelli, G., & Firmani, C. 2003, ApJ, 598, 36
Avila-Reese, V. Colín, P., González-Samaniego, A., Firmani, C., Velázquez, H., Valenzuela, O., & Ceverino, D. 2011, ApJ, 736, 134
Benson, A. J., Farahi, A., Cole, S., et al. 2013, MNRAS, 428, 1774
Bode, P., Ostriker, J. P., & Turok, N. 2001, ApJ, 556, 93
Boyarsky, A., Ruchayskiy, O., & Shaposhnikov, M. 2009, Annual Review of Nuclear and Particle Science, 59, 191
Brooks, A. 2014, Annalen der Physik 264, 294
Bullock, J.S., Dekel, A., Kolatt, T.S., Kravtsov, A.V., Klypin, A.A., Porciani, C., & Primack, J.R. 2001, ApJ, 555, 240
Christensen, C., Quinn, T., Governato, F., et al. 2012, MNRAS, 425, 3058
Cloet-Osselaer, A., De Rijcke, S., Vandenbroucke, B., et al. 2014, MNRAS, 442, 2909
Cole, A. A., Weisz, D. R., Dolphin, A. E., et al. 2014, ApJ, 795, 54
Colín, P., Avila-Reese, V., & Valenzuela, O. 2000, ApJ, 542, 622
Colín, P., Avila-Reese, V., Valenzuela, O., & Firmani, C. 2002, ApJ, 581, 777
Colín, P., Avila-Reese, V., Vázquez-Semadeni, E., Valenzuela, O., & Ceverino, D. 2010, ApJ, 713, 535
Colín, P., Valenzuela, O., & Avila-Reese, V. 2008, ApJ, 673, 203
Dalla Vecchia, C., & Schaye, J. 2012, MNRAS, 426, 140
Del Popolo, A., Lima, J. A. S., Fabris, J. C., & Rodrigues, D. C. 2014, JCAP, 4, 21
de Vega, H. J., Salucci, P., & Sanchez, N. G. 2014, MNRAS, 442, 2717
Dodelson, S., & Widrow, L. M. 1994, Physical Review Letters, 72, 17
Ellis, J., Kim, J. E., & Nanopoulos, D. V. 1984, Physics Letters B, 145, 181
Ferland, G.J., Korista, K.T., Verner, D.A., Ferguson, J.W., Kingdon, J.B., & Verner, E.M. 1998, PASP, 110, 761
Ferrero, I., Abadi, M. G., Navarro, J. F., Sales, L. V., & Gurovich, S. 2012, MNRAS, 425, 2817
Firmani, C., D'Onghia, E., Avila-Reese, V. Chincarini, G., Hernndez, X. 2000, MNRAS, 315, L29
Frenk, C. S., & White, S. D. M. 2012, Annalen der Physik, 524, 507
Gao, L., & Theuns, T. 2007, Science, 317, 1527
Gao, L., Theuns, T., & Springel, V. 2014, arXiv:1403.2475
González-Samaniego, A., Colín, P., Avila-Reese, V., Rodríguez-Puebla, A., & Valenzuela, O. 2014, ApJ, 785, 58 (G+2014)
Götz, M., & Sommer-Larsen, J. 2003, Ap&SS, 284, 341
Geha, M., Blanton, M. R., Masjedi, M., & West, A. A. 2006, ApJ, 653, 240
Geha, M., Blanton, M. R., Yan, R., & Tinker, J. L. 2012, ApJ, 757, 85
Governato, F., Weisz, D., Pontzen, A., et al. 2014, arXiv:1407.0022
Haardt, F., & Madau, P. 1996, ApJ, 461, 20
He, Y., & Lin, W. 2013, Phys. Rev. D, 87, 063520
Herpich, J., Stinson, G. S., Macciò, A. V., et al. 2014, MNRAS, 437, 293
Hogan, C. J., & Dalcanton, J. J. 2000, Phys. Rev. D, 62, 063511
Hopkins, P. F., Quataert, E., & Murray, N. 2012, MNRAS, 421, 3522
Hopkins, P. F., Kereš, D., Oñorbe, J., et al. 2014, MNRAS, 445, 581
Kang, X., Macciò, A. V., & Dutton, A. A. 2013, ApJ, 767, 22
Kennedy, R., Frenk, C., Cole, S., & Benson, A. 2014, MNRAS, 442, 2487
Klypin, A.A., & Holtzman, J. 1997, preprint (astro-ph/9712217)
Klypin, A., Gottl´ober, S., Kravtsov, A. V., et al. 1999, ApJ, 516, 530
Klypin, A., Karachentsev, I., Makarov, D., & Nasonova, O. 2014, arXiv:1405.4523
Klypin, A.A., Kravtsov, A.V., Bullock, J.S., & Primack, J.R. 2001, ApJ, 554, 903
Knebe, A., Devriendt, J. E. G., Mahmood, A., & Silk, J. 2002, MNRAS, 329, 813
Knebe, A., Devriendt, J. E. G., Gibson, B. K., & Silk, J. 2003, MNRAS, 345, 1285
Kolb, E., & Turner, M. 1990, The Early Universe, Addison-Wesley, Redwood City, CA, Frontiers in Physics, 69
Kravtsov, A.V., Klypin, A.A., & Khokhlov, A.M., 1997, ApJS, 111, 73
Kravtsov, A.V. 2003, ApJ(Letters), 590, 1
Kuhlen, M., Krumholz, M. R., Madau, P., Smith, B. D., & Wise, J. 2012, ApJ, 749, 36
Libeskind, N.I., Di Cintio, A., Knebe, A., Yepes, G., Gottl´ober, S., Steinmetz, M., Hoffman, Y., & Martinez-Vaquero, L.A. 2013, PASA, 30, 39
Lin, W. B., Huang, D. H., Zhang, X., & Brandenberger, R. 2001, Physical Review Letters, 86, 954
Lovell, M. R., Eke, V., Frenk, C. S., et al. 2012, MNRAS, 420, 2318
Lovell, M.R., Frenk, C.S., Eke, V.R., Jenkins, A., Gao, L, & Theuns, T. 2014, MNRAS, 439, 300 (L2014)
Macciò, A. V., & Fontanot, F. 2010, MNRAS, 404, L16
Macciò, A. V., Paduroiu, S., Anderhalden, D., Schneider, A., & Moore, B. 2012, MNRAS, 424, 1105
Menci, N., Fiore, F., & Lamastra, A. 2012, MNRAS, 421, 2384
Miller, G.E., & Scalo, J.M. 1979, ApJS, 41, 513
Moroi, T., Murayama, H., & Yamaguchi, M. 1993, Physics Letters B, 303, 289
Munshi, F., Governato, F., Brooks, A. M., et al. 2013, ApJ, 766, 56
Narayanan, V. K., Spergel, D. N., Davé, R., & Ma, C.-P. 2000, ApJ, 543, L103
Pagels, H., & Primack, J. R. 1982, Physical Review Letters, 48, 223
Papastergis, E., Martin, A. M., Giovanelli, R., & Haynes, M. P. 2011, ApJ, 739, 38
Papastergis, E., Giovanelli, R., Haynes, M. P., & Shankar, F. 2014, arXiv:1407.4665
Planck Collaboration, Ade, P. A. R., Aghanim, N., et al. 2014, A&A, 571, AA16
Rodríguez-Puebla, A., Avila-Reese, V., & Drory, N. 2013, ApJ, 773, 172
Sawala, T., Scannapieco, C., Maio, U., & White, S. 2010, MNRAS, 402, 1599
Sawala, T., Frenk, C. S., Fattahi, A., et al. 2014a, arXiv:1406.6362
Sawala, T., Frenk, C. S., Fattahi, A., et al. 2014b, arXiv:1404.3724
Schneider, A., Smith, R.E., Macció, A., & Ben Moore. 2012, MNRAS, 424, 684
Schneider, A., Smith, R. E., & Reed, D. 2013, MNRAS, 433, 1573
Schneider, A., Anderhalden, D., Macciò, A. V., & Diemand, J. 2014, MNRAS, 441, L6
Shi, X., & Fuller, G. M. 1999, Physical Review Letters, 82, 2832
Smith, R. E., & Markovic, K. 2011, Phys. Rev. D, 84, 063507

Spergel, D. N., & Steinhardt, P. J. 2000, Physical Review Letters, 84, 3760
Sommer-Larsen, J., & Dolgov, A. 2001, ApJ, 551, 608.
Stinson, G. S., Brook, C., Macciò, A. V., et al. 2013, MNRAS, 428, 129
Trujillo-Gomez, S., Klypin, A., Colin, P., et al. 2013, arXiv:1311.2910
Viel, M., Lesgourgues, J., Haehnelt, M.G., Matarrese, S., & Riotto, A. 2005, Phys. Rev. D71, 063534
Viel, M., Becker, G.D., Bolton, J.S., & Haehnelt, M.G. 2013, Phys. Rev. D, 88d, 3502
Wang, j., & White, S.D.M. 2007, MNRAS, 380, 93
Weinberg, D. H., Bullock, J. S., Governato, F., Kuzio de Naray, R., & Peter, A. H. G. 2013, arXiv:1306.0913
Weisz, D. R., Dolphin, A. E., Skillman, E. D., et al. 2014, ApJ, 789, 147
Yoshida, N., Springel, V., White, S. D. M., & Tormen, G. 2000, ApJ, 544, L87
Zavala, J., Jing, Y. P., Faltenbacher, A., et al. 2009, ApJ, 700, 1779